Wide color-range tunable and low roll-off fluorescent organic light emitting devices based on double undoped ultrathin emitters

Ting Xu [a], Meijun Yang [b], Jun Liu [b], Xinkai Wu [b], Imran Murtaza [c], Gufeng He [b, *], Hong Meng [a, **]

[a] School of Advanced Materials, Peking University Shenzhen Graduate School, Peking University, Shenzhen 518055, China
[b] National Engineering Lab for TFT-LCD Materials and Technologies, Department of Electronic Engineering, Shanghai Jiao Tong University, Shanghai, 200240, China
[c] Key Laboratory of Flexible Electronics and Institute of Advanced Materials, Jiangsu National Synergistic Innovation Centre for Advanced Materials, Nanjing Tech University, Nanjing, 211816, China

ABSTRACT

We demonstrated a novel wide color-range tunable, highly efficient and low efficiency roll-off fluorescent organic light-emitting diode (OLED) using two undoped ultrathin emitters having complementary colors and an interlayer between them. The OLED can be tuned to emit sky blue (0.22, 0.30), cold white (0.29, 0.33), warm white (0.43, 0.42) and yellow (0.40, 0.45) according to the Commission Internationale de L'Eclairage (CIE) 1931 (x, y) chromaticity diagram. The device fabrication was simplified by eliminating doping process in the emission layers. The influence of interlayer thickness on luminous efficiency, efficiency roll-off and color tuning mechanism is thoroughly studied. The recombination zone is greatly broadened in the optimized device, which contributes to stable energy transfer to both emitters and suppressed concentration quenching. With a threshold voltage of 2.82 V, the color tunable organic light emitting diode (CT-OLED) shows a maximum luminance of 39,810 cd/m^2, a peak external quantum efficiency (EQE) 6% and the efficiency roll-off as low as 11.1% at the luminance from 500 cd/m^2 to 5000 cd/m^2. This structure of CT-OLED has great advantages of easy fabrication and low reagent consumption. The fabricated CT-OLEDs are tunable from cold white (0.30, 0.36) to warm white (0.43, 0.42) with correlated color temperature (CCT) 6932 K and 3072 K, respectively, demonstrating that our proposed approach helps to meet the need for lighting with various CCTs.

© 2016 Elsevier B.V. All rights reserved.

1. Introduction

In the past three years, organic light-emitting diode (OLED) technology has played a unique role in solid-state lighting and flat-panel displays market due to their remarkable properties such as impressive color rendering, wide viewing angles, ease of fabricating large-area panel and high compatibility with flexible substrates [1,2]. Since the demonstration of first efficient OLED by Tang in 1980s [3], tremendous progress has been accomplished in this field. For example, the internal quantum efficiency of OLEDs possible close to 100% has been achieved by using phosphorescent and thermally activated delayed fluorescence emitters (TADF) [4,5]. White organic light-emitting diodes (WOLEDs) have been successfully fabricated by using vacuum deposited or solution processed organic thin film emissive layer (EML) having complementary colors [6,7]. However, the OLED based products are still very expensive and unaffordable to most of the consumers. So it is desperately demanded to simplify the OLED device structure and process to lower the fabrication cost [8]. Color tunable organic light emitting diode (CT-OLEDs) firstly reported by Forrest [9], which show potential to applied in display and lighting [10]. Some previous works on CT-OLEDs showed that assembling materials, including mixing of rare elements in complexes [11,12] and adjusting the Eu^{3+} complex ratio in the matrix [13], can be used for CT-OLEDs by controlling intensity ratio of the different spectral peaks and reducing back-transfer quenching effect. Moreover, driving separate light-unit device based on complementary light theory and micro-cavity effects [14] is an effective route to realize

CT-OLEDs, as Burrows [9] and Kwok [15] used the stacked OLED structure and alternating current driven system [16]. Besides those complicated device architectures and processing methods [17,18], inserting an interlayer [19] in two or three complementary emitting layers is also an important and effective route to achieve CT-OLEDs. For example, Lee [20] group realized a color-shifted device by utilizing a CdSe end-capped ZnS quantum dot interlayer to control electron transport. Jou [21] group realized a wide color range device by using 1,3,5-tris(*N*-phenylbenzimidazol-2-yl) benzene (TPBi) as a hole modulating interlayer inserted in three EMLs to modulate hole carrier distribution. Yook group [22] also achieved a simple CT-OLED with limited color adjustable range whose CIE coordinates vary from blue-green light with CIE (0.24, 0.43) to orange light (0.43, 0.39)[23] by inserting a mixed interlayer of 4.4′,4″tris (*N*-carbazolyl)triphenylamine (TCTA) and 3-(biphenyl-4-yl)-4-pheny-5-(4-*tert*-butylphenyl)-1,2,4-triazole (TAZ) between yellow and blue EMLs, to control hole and electron transport. However, the emitters of CT-OLEDs generally consist of double or triple layers of doped EML which leads to complicated fabrication process due to the difficulties in precisely controlling the doping concentration [24]. Moreover, organic EML materials are especially expensive. Thus, there is an increasing demand for CT-OLEDs consuming less organic EML materials to obtain wider color-tunable range, high efficiency and reduced roll-off with easy fabrication process [25,26]. The correlated color temperature (CCT), which is closely related to the relative amount of blue and yellow emission in white spectrum, is of special interest in designing WOLEDs with reports supporting significant physiological impact of blue and yellow emission in lightings on human beings [27–29].

In this work, we report a novel fluorescent CT-OLEDs opening new horizons of double undoped ultrathin yellow and blue emissive layers regularly applied in fabricating white OLEDs [30], which consume a very small amount of organic EML material in device fabrication process and can be tunable over warm white color and cold white color with correlated color temperature (CCT) of 6932 K and 3072 K, respectively. *p*-bis(p-*N*,*N*-di-phenyl-aminostyryl)benzene (DSA-ph) is used as blue emitter which is a promising fluorescent material and has been widely studied [31], whereas, 2,8-di (*t*-butyl)-5,11-di [4 (*t*-butyl)phenyl]-6,12-diphenylnaphthacene (tetra (t- butyl)rubrene) (TBRb) serves as the yellow fluorescent emissive material. In particular, the electroluminescence (EL) spectrum of DSA-ph overlaps the absorption spectrum of TBRb very well, which ensures efficient energy transfer from DSA-ph to TBRb. 2-methyl-9,10-di (2-naphthyl) anthracene (MADN) is inserted between the two emitters as an interlayer of suitable thickness in order to tune the energy transfer, which affects the illuminant color, between blue and yellow emitters. In addition, N, N,'-bis-(1-*naphthyl*)-N, N'-diphenyl-1.1'-biphenyl-4.4'-diamine (NPB) and 1,3,5-Tris (*N*-phenylbenzimidazol-2-yl) benzene (TPBi) as hole transporting layer (HTL) and electron transporting layer (ETL), respectively, are also applied. Relatively thicker TPBi ETL helps to prevent exciton quenching by electrode, moreover, optimizing TPBI thickness help to improve the carrier injection and transport to achieve high efficient OLED. The optimized CT-OLED shows wide color-range tunability, high efficiency and reduced roll-off at high brightness.

2. Experiment details

All devices were fabricated on glass substrates with patterned indium-tin-oxide (ITO) anode having a sheet resistance of 15 Ω/square. The substrates were subjected to a routine cleaning process with rinsing in deconex 12Pa-A, deionized water, acetone, isopropanol via ultra-sonifications for 15 min each and then dried with nitrogen gun and finally treated in a UV–ozone chamber for 15 min. The multi-functional layers including inorganic buffer layers, organic layers and cathode materials were sequentially deposited on the substrates without breaking vacuum (~5.0 × 10^{-6} Torr). The evaporation rates of MoO_3, organic layers, LiF and Al were about 0.1 Å/s, 1 Å/s, 0.1 Å/s and 5 Å/s, respectively. The deposition rates were monitored in-situ with quartz crystals. The actual device area defined by the overlap of the ITO anode and the Al cathode was 3 mm × 3 mm.

The basic structure of the devices is ITO/MoO_3 (1 nm)/NPB (60 nm)/TBRb (0.3 nm)/MADN (y nm)/DSA-ph (0.2 nm)/TPBi (x nm)/LiF (1 nm)/Al (100 nm). The Schematic and energy level diagrams of the fabricated devices are shown in Fig. 1 and schematic parameters are given in Table 1. MoO_3 and NPB act as hole injection layer (HIL) and hole transporting layer (HTL), respectively, whereas LiF and TPBi act as electron injection layer (EIL) and electron transporting layer (ETL), respectively. Devices A, B, C, D and E are OLEDs with TBRb as yellow emitter. Devices A, D, E have fixed MADN thickness and variable TPBi thickness (25, 35, 45 nm), to prevent exciton quenching, whereas devices A, B and C have variable MADN thicknesses (10, 15, 20 nm) and fixed TPBi thickness. The molecular structures of NPB, TPBi, TBRb, DSA-ph and MADN are shown in Fig. 2.

The current density-voltage-luminance (J-V-L), current efficiency-current density (CE-J) characteristics and the color coordinates of unpackaged devices were measured with a computer controlled Keithley 2400 Source Meter and Topcon BM-7A Luminance Colorimeter. The spectra of the devices were measured with Ocean Optics Maya 2000-PRO spectrometer. All measurements were carried out at room temperature and under ambient conditions without encapsulation.

3. Results and discussion

Förster resonance energy transfer [27] is often used to describe the hopping of an exciton between identical molecules [32], but can also be used to describe the energy transfer between different species [33,34]. The range of interaction varies depending on the strength of the interaction from short range (nearest neighbors) to ~10 nm [28]. Förster energy transfer and Dexter energy transfer processes are theoretically [35–37] and experimentally [38,39] proven, and are widely accepted and applied in interpretation of energy transfer process in organic semiconductor devices [40,41]. The interesting Förster energy transfer process (within the range ~10 nm), in our CT-OLEDs is highlighted in Fig. 3. In our designed OLED device, the yellow emitter, TBRb, has strong absorption between 450 nm and 550 nm, while DSA-ph has a peak emission at 470 nm and a shoulder at 502 nm (Supporting Information (SI):SI. Fig. 1.). The good overlap between the emission of DSA-ph and the absorption of TBRb shall lead to efficient Förster energy transfer from DSA-ph to TBRb when two different molecules are near enough to ~10 nm.

However, in order to obtain wide color-range tunable OLED device, thick MADN interlayer (≥10 nm) is designed into the device to realize two functions. Firstly, thick MADN efficiently captures the injected holes and electrons just similarly acting as a host in host–guest doping system tending to transfer more energy to DSA-ph rather than TBRb as S1 energy level of MADN is much closer to DSA-ph, and the lower molecular orbit of DSA-ph is more stable than MADN. Secondly, Förster resonance energy transfer between DSA-ph and TBRb is partly restricted if the interlayer is thicker than 10 nm [42]. The energy transfer process among MADN, TBRb and DSA-ph, discussed above, is illuminated in Fig. 3.

Schematic energy level diagram of the device can be seen in Fig. 1. The corresponding hole (or electron) injection barrier was determined by the energy level difference between the work
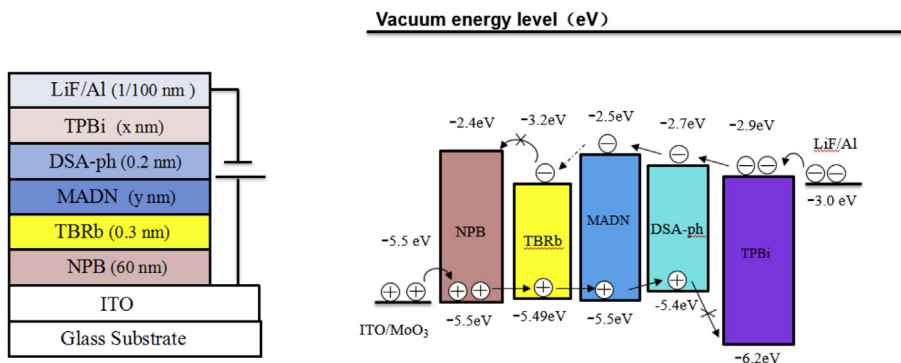
Fig. 1. Schematic parameters and energy level diagrams of the fabricated device.

Table 1
Structures of the OLED devices.

Devices	Device structure: ITO/MoO$_3$ (1 nm)/NPB(60 nm)/TBRb(0.3 nm)/MADN (x nm)/DSA-ph (0.2 nm)/TPBi(y nm)/LiF(1 nm)/Al (100 nm)
Device A	MADN (10 nm)/DSA-ph (0.2 nm)/TPBi(25 nm)
Device B	MADN (15 nm)/DSA-ph (0.2 nm)/TPBi(25 nm)
Device C	MADN (18 nm)/DSA-ph (0.2 nm)/TPBi(25 nm)
Device D	MADN (10 nm)/DSA-ph (0.2 nm)/TPBi(35 nm)
Device E	MADN (10 nm)/DSA-ph (0.2 nm)/TPBi(45 nm)/

Device A, B, C with fixed TPBi thickness and variable MADN thickness.
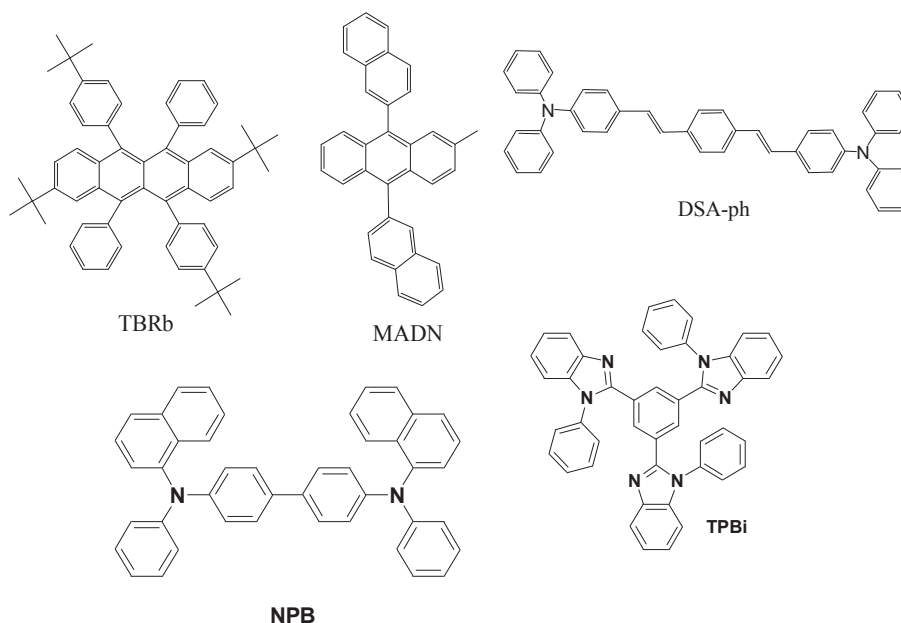Device A, D, E with fixed MADN thickness and variable TPBi thickness.

Fig. 2. Chemical structures of organic materials used to fabricate color-tunable devices.

function of the electrode and the highest occupied molecular orbital (HOMO) of NPB (−5.5 eV) [43] or the lowest unoccupied molecular orbital (LUMO) of TPBi (−2.9 eV) [23]. The current density-voltage-luminance (J-V-L) and current efficiency-current density characteristics of devices A to E are shown in Fig. 4 and Table 2.

The increase in current density with respect to the applied voltage gets slow from device A to device C due to the increase in MADN interlayer thickness from 10 nm to 18 nm. The turn-on voltages of the devices A, B and C are about 2.82 V, 2.90 V and 3.20 V, respectively. Device A with the thinnest interlayer has the

lowest turn-on voltage and the highest current density, and carriers can be readily transported into DSA-ph and TBRb through thin MADN interlayer in the device A. The turn-on voltage of device A is only 2.82 V and the maximum current efficiency is 5.72 cd/A while reaching the maximum external quantum efficiency (EQE) 1.87%, a bit lower than that of device B and C, with the maximum current efficiency 6.22 cd/A (EQE 2.007%) and 6.71 cd/A (EQE 2.126%), respectively. It may be related to the smaller amount of MADN in device A than in devices B and C, to capture the injected holes and electrons, and then transfer the energy to the emitting layers. The luminance of the EML reaches the peak value at 34,700 cd/m^2 as the
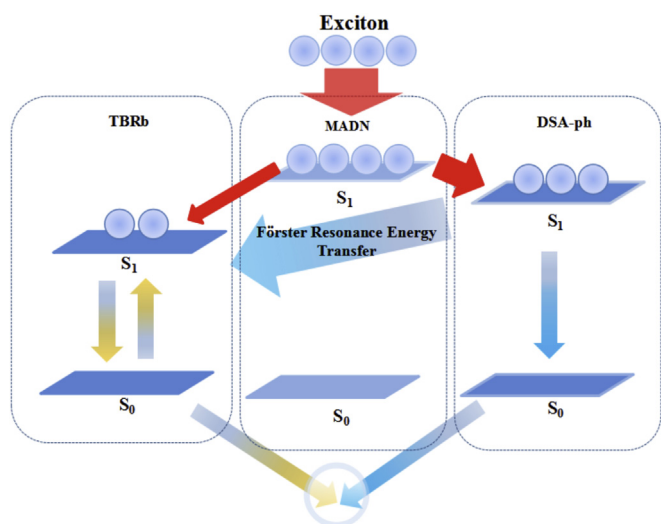
Fig. 3. Schematic diagram showing the energy transfer process for emitting light with different colors.

MADN interlayer increases to 15 nm and slightly declines to 34,090 cd/m^2 as the MADN interlayer increases to 18 nm. In order to further explore the device working mechanism, we changed the TPBi thickness (25 nm, 35 nm and 45 nm) which acts as an ETL. Comparing with reference device A, devices D and E show generally better performance with the maximum current efficiencies of 5.66 cd/A (EQE 1.889%) and 6.16 cd/A (EQE 2.024%), respectively. Moreover, the designed CT-OLEDs show warm white at 500 cd/m^2 with the maximum EQE as a whole.

Owing to the fact that holes have higher mobility than electrons, they reach the cathode prior to electrons leading to quenching by cathode. Therefore, the increase in TPBi thickness moves the exciton recombination zone far away from the cathode, which helps to prevent exciton quenching, as shown in Fig. 4 (c). Moreover, the ultrathin emitters with high carrier concentration in the recombination zone lead to a more serious concentration-quenching [44] and this condition is exacerbated in higher carrier concentration resulting in strong efficiency roll-off at high luminance in designed OLEDs. In the devices, most excitons are formed on the interlayers and transfer energy to the blue and yellow emitters. The recombination zone is greatly broadened as the interlayer thickness increasing among device A, B and C, and the exciton concentration decreases. Thus, improved luminous efficiency is obtained and the efficiency roll-off can be suppressed.
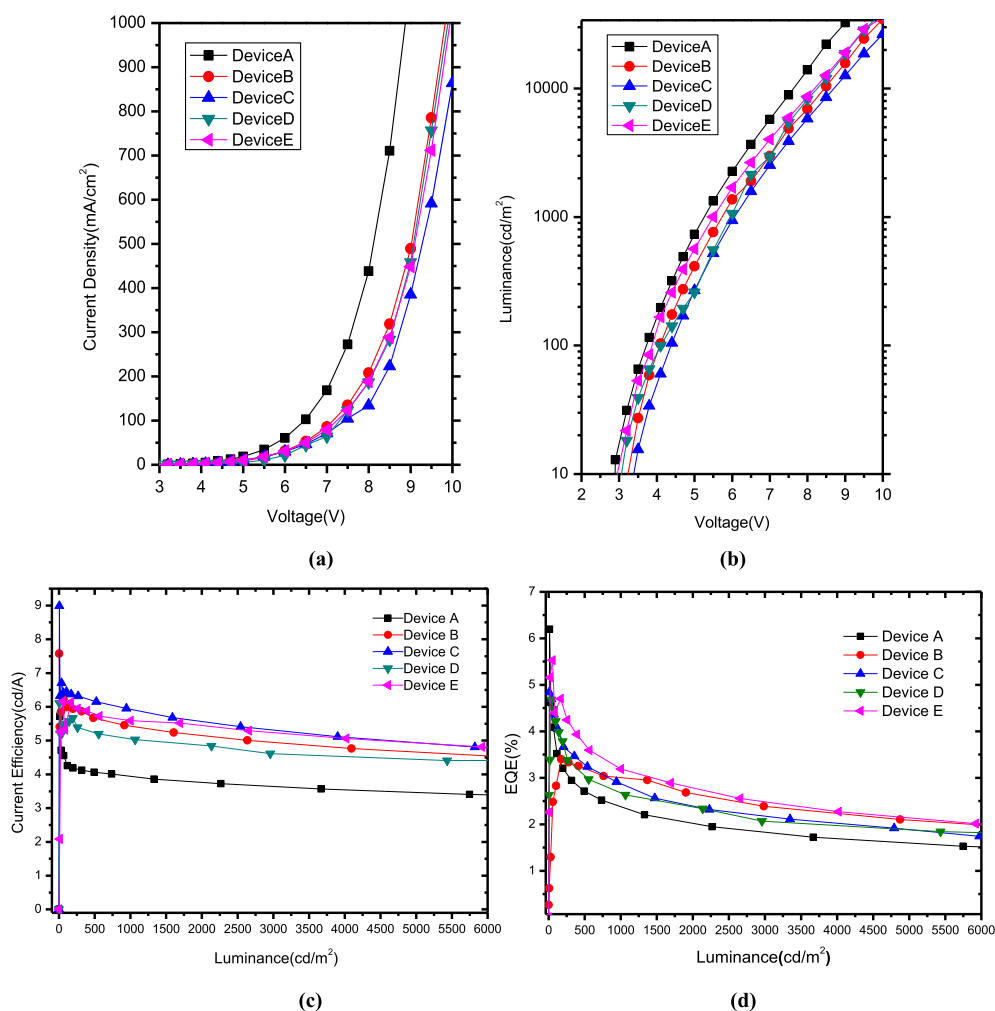

(a)

(b)

(c)

(d)

Fig. 4. (a) Voltage-current density (b) Voltage-luminance characteristics of devices (c) Current efficiency-luminance decay characteristics of devices (d) EQE-luminance characteristics of devices.

Table 2
Summary of CT-OLEDs performance.

Device	$V_{turn-on}$[a] (V)	L_{max} (cd/m^2)	η_c (cd/A) (EQE (%))		CIE $_p$ (x, y)[b] (CCT)	CIE at 500 cd/m^2 (x, y) (CCT)	Roll-off (%) 500–5000 cd/m^2
			Max	at 500 cd/m^2			
A	2.82	32,420	5.72 (1.871)	4.06 (1.328)	0.27, 0.30 (10,408 K)	0.47, 0.41 (2450 K)	16.1
B	2.90	34,700	6.22 (2.007)	5.67 (2.007)	0.43, 0.41 (3105 K)	0.41, 0.38 (3249)	16.0
C	3.20	34,090	6.71 (2.126)	5.29 (1.764)	0.40, 0.40 (3656 K)	0.46, 0.42 (2680)	21.1
D	2.83	39,810	5.66 (1.889)	5.19 (1.732)	0.43, 0.41 (3105 K)	0.46, 0.42 (2680 K)	11.1
E	2.83	36,040	6.16 (2.024)	5.72 (1.88)			19.1

[a] Turn-on voltage is defined as the luminance of OLEDs reaching 1 cd/m^2.
[b] CIE $_p$ is the CIE at peak current efficiency.

Therefore, the efficiency roll-off of all designed CT-OLEDs are lower than 21.1% and the best efficiency roll-off is as low as 11.1% in device D at the luminance from 500 cd/m^2 to 5000 cd/m^2 due to the thickner TPBi preventing exciton quenching by lowering the high concentration of excitons, which is relatively advisable compared with previously reported CT-OLEDs [45–47] showing the best efficiency roll-off more than 30% from 500 cd/m^2 to 5000 cd/m^2. Although exciton density in the ultrathin emitting layers seem to be significantly high, the exciton recombination luminescence process also vary fast to lower the exciton density. Triplet state quenched also reduce as the exciton density reduce by thicker MADN suppressing efficiency roll-off by managing the interlayer [48] and host properties as showing in SI: Fig. 4.

Under low applied electric field, holes are injected from the anode (ITO/MoO$_3$) and easily transported to DSA-ph EML since the HOMO of NPB, TBRb, MADN and DSA-ph are quite close while electrons are injected from the cathode (LiF/Al) and tend to be slightly confined in DSA-ph EML since the LUMO levels of TPBi, DSA-ph, MADN and TBRb are −2.9 eV, −2.7 eV, −2.5 eV and −3.2eV respectively. There are two small barriers (0.2 eV) transporting electrons to yellow EML. Moreover, electrons cannot be transported easily from MADN to TBRb in device A and tend to be located in MADN interlayer. Especially in low electron density at low driving voltage, tunneling the barrier between interface of MADN and TBRb to emit yellow color is not remarkable, hence excitons in MADN transfer energy to DSA-ph layer, which leads to some blue emission from DSA-ph. Further, the LUMO energy gap between MADN and NPB is only 0.1 eV and the TBRb is sufficiently thin (0.3 nm).

However, at low bias voltage, only few electrons are injected through the interlayer while most of the electrons are blocked in the blue EML by the interlayer. Holes and electrons recombine and form excitons mainly at the interface of the interlayer and the blue EML. Why the CIE coordinate is highly voltage dependent yellow shifted as the applied voltage increases? This is because the electron is known to be the minor carrier in typical OLED devices due to its intrinsically low mobility [26], although this would dramatically increase as the applied voltages increases. The increasing number of electrons are transported to the yellow-emissive TBRb zone resulting in a higher probability of recombination, showing that more recombinations must be taking place in the yellow-emissive zones. Moreover, Förster resonance energy transfer effect is remarkably strengthened by increasing applied voltage due to higher concentration of excitons leading to a more yellow-emission as observed. Therefore, as shown in Table 3 and Fig. 5, the device A initially shows a predominantly blue-emission spectrum at 2.9 V with CIE coordinates of (0.204, 0.29) (21,996K) with 4.956 cd/m^2, turns to pure white (0.301, 0.362) (6869 K) at 3.8 V with 58.81 cd/m^2, becomes yellow white (0.366, 0.376) (4396 K) at 4.4 V with

174.5 cd/m^2 and then gradually becomes yellow (0.435, 0.417) (3072 K) at 8.0 V with 6910 cd/m^2. Thus, there is an increase from 4.956 to 6910 cd/m^2 relative to the increase in applied voltage from 3.2 to 8 V in device A. The device B initially shows a predominantly blue-emission spectrum at 2.9 V with CIE coordinates of (0.269, 0.269) (13,104 K) with 12.9 cd/m^2, turns to pure white (0.33, 0.34) (5606 K) at 3.2 V with 31.31 cd/m^2, becomes yellow white (0.445, 0.404) at 4.1 V with 197 cd/m^2 and then gradually becomes yellow (0.469, 0.442) (2728 K) at 8.0 V with 13,940 cd/m^2. Thus, there is an increase from 12.9 to 13,940 cd/m^2 relative to the increase in applied voltage from 3.2 to 8 V in device B. In the device C, initially CT-OLED shows a predominantly blue-emission spectrum at 2.9 V with CIE coordinates of (0.206.0.338) (14,337 K) with 4.543 cd/m^2, turns to white (0.338.0.378) (5327 K) at 3.8 V with 41.35 cd/m^2, becomes yellow white (0.428.0.415) (3186 K) at 4.4 V with 207 cd/m^2 and then gradually becomes yellow (0.474, 0.43) (2563 K) at 8.0 V with 5973 cd/m^2. Thus, there is an increase from 4.956 to 6910 cd/m^2 relative to the increase in applied voltage from 3.2 to 8 V in device C. The best color temperature tunable range of designed CT-OLEDs is from 14,337 K to 2563 K by increasing voltage. The fabricated CT-OLEDs are tunable from cold white (0.30, 0.36) to warm white (0.43, 0.42) with correlated color temperature (CCT) 6932 K and 3072 K, respectively.

As the MADN thickness increase from 10 nm in device A to 18 nm in device C, the color range tends to enlarge especially in yellow region as shown in Fig. 5 mainly due to more excitons located in thicker MADN and limited electrons transport in the thicker MADN interlayer resulting in the improvement of current efficiency as shown in SI: Figs. 2 and 3. At high bias voltage, more electrons overcome the barrier and enter the yellow-emissive zone to recombine with holes and emit yellow light. This phenomenon also contributes to the tunable color-range enlargement to yellow region. In addition, we can hardly see the blue emission from MADN as shown in Fig. 6, which is located at 430 nm, indicating that the energy transfer from MADN to DSA-ph and TBRb is quite efficient. In the device A, B and C, most excitons are formed on the interlayers and transfer energy to the blue and yellow emitters. Moreover, the molecules in the ultrathin emitters are limited, leading to high concentration in the recombination zone [28] and the concentration-quenching gets more pronounced at high luminance, resulting in strong efficiency roll-off. The recombination zone is highly broadened by optimized thicker interlayer and the exciton concentration decreases. Thus, improved luminous efficiency is obtained and the efficiency roll-off can be suppressed. A peak EQE 6% at low voltage of the proposing fluorescence CT-OLEDs are not remarkable due to thin emitting zone, ordinary functional materials and the limited EQE of fluorescence luminescent materials, even so, it is possible to further improve the efficiency by

Table 3
The Luminance and CIE of device A, B and C change with voltage.

| Voltage(V)	Luminance (cd/m²) and CIE (x, y)					
	Device A		Device B		Device C	
2.9	4.956	0.204, 0.29	12.9	0.269, 0.296	4.543	0.206, 0.338
3.2	8.846	0.22, 0.31	31.31	0.33, 0.34	7.173	0.237, 0.335
3.5	27.26	0.25, 0.34	65.49	0.388, 0.37	41.35	0.338, 0.378
3.8	58.81	0.301, 0.362	115.5	0.424, 0.387	72.9	0.375, 0.392
4.4	174.5	0.366, 0.376	317.9	0.46, 0.412	207	0.428, 0.415
5	413.8	0.408, 0.382	736	0.476, 0.423	538.3	0.458, 0.423
6.5	1904	0.432, 0.410	3670	0.487, 0.43	2229	0.479, 0.427
8	6910	0.435, 0.417	13940	0.469, 0.442	5973	0.474, 0.43
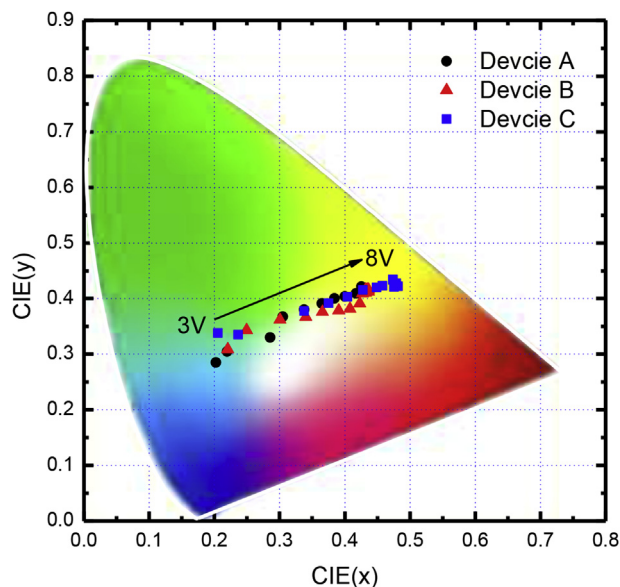
Fig. 5. The variation of CIE color coordinates of device A, B and C varying with voltages.
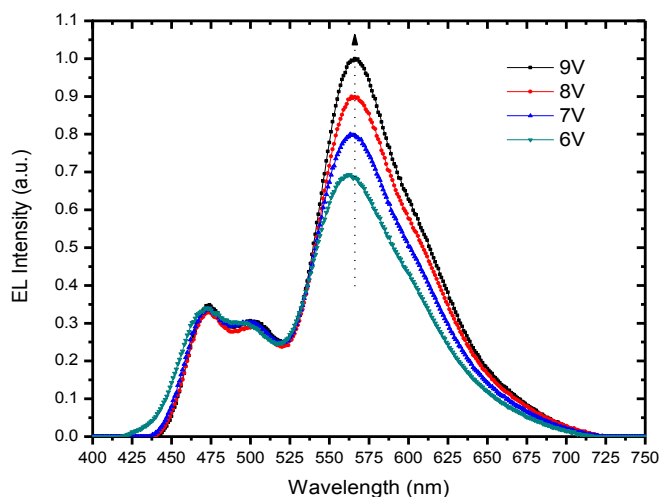

Fig. 6. The normalized EL spectra (at blue peak) of OLED Device A at 6–9 V.

using novel phosphorescent [49] or thermally activated delayed fluorescence [50] emitters in this structure CT-OLED.

4. Conclusion

In summary, wide color-range tunable, highly efficient and low roll-off efficiency fluorescent CT-OLEDs have been demonstrated based on two undoped ultrathin emitters with complementary colors and an interlayer between them. With a threshold voltage of 2.82 V, the CT-OLEDs show a maximum luminance of 39810 cd/m², the peak current efficiency of 8.99 cd/A, a peak EQE 6% and the efficiency roll-off as low as 11.1% at the luminance from 500 cd/m² to 5000 cd/m², which can be tuned to emit sky blue (0.22, 0.30), cold white (0.29, 0.33), warm white (0.43, 0.42) and yellow (0.40, 0.45) light. As the structure of the device is highly simplified with ultrathin and undoped emitters, it shows great advantages of easy fabrication and low reagent consumption. The fabricated CT-OLEDs are tunable from cold white (0.30, 0.36) to warm white (0.43, 0.42) with correlated color temperature (CCT) 6932 K and 3072 K, respectively, demonstrating that our proposed approach helps to meet the need for lighting with various CCTs. These encouraging results indicate that OLEDs incorporating undoped ultrathin emitters with desired chromaticity characteristics can be easily fabricated and are promising candidates for color tunable solid-state lighting applications.

Appendix A. Supplementary data

Supplementary data related to this article can be found at http://dx.doi.org/10.1016/j.orgel.2016.06.014.

References

[1] Z.B. Wang, M.G. Helander, J. Qiu, D.P. Puzzo, M.T. Greiner, Z.M. Hudson, S. Wang, Z.W. Liu, Z.H. Lu, Unlocking the full potential of organic light-emitting diodes on flexible plastic, Nat. Photonics 5 (12) (2011) 753–757.
[2] S. Reineke, F. Lindner, G. Schwartz, N. Seidler, K. Walzer, B. Lussem, K. Leo, White organic light-emitting diodes with fluorescent tube efficiency, Nature 459 (7244) (2009) 234–238.
[3] C.W. Tang, S.A. VanSlyke, Organic electroluminescent diodes, Appl. Phys. Lett. 51 (12) (1987) 913–915.
[4] M.A. Baldo, D.F. O'Brien, Y. You, A. Shoustikov, S. Sibley, M.E. Thompson, S.R. Forrest, Highly efficient phosphorescent emission from organic electro-luminescent devices, Nature 395 (6698) (1998) 151–154.
[5] H. Uoyama, K. Goushi, K. Shizu, H. Nomura, C. Adachi, Highly efficient organic light-emitting diodes from delayed fluorescence, Nature 492 (7428) (2012) 234–238.
[6] J. Kido, M. Kimura, K. Nagai, Multilayer white light-emitting organic electro-luminescent device, Science 267 (5202) (1995) 1332–1334.
[7] T. Chiba, Y.-J. Pu, J. Kido, Solution-processed white phosphorescent tandem organic light-emitting devices, Adv. Mater. 27 (32) (2015) 4681–4687.
[8] F. Ventsch, M.C. Gather, K. Meerholz, Towards organic light-emitting diode microdisplays with sub-pixel patterning, Org. Electron. 11 (1) (2010) 57–61.

[9] P.E. Burrows, S.R. Forrest, S.P. Sibley, M.E. Thompson, Color-tunable organic light-emitting devices, Appl. Phys. Lett. 69 (20) (1996) 2959.

[10] Z. Shen, P.E. Burrows, V. Bulović, S.R. Forrest, M.E. Thompson, Three-color, tunable, organic light-emitting devices, Science 276 (5321) (1997) 2009–2011.

[11] R. Reyes, M. Cremona, E.E.S. Teotonio, H.F. Brito, O.L. Malta, Voltage color tunable OLED with (Sm,Eu)-beta-diketonate complex blend, Chem. Phys. Lett. 396 (1–3) (2004) 54–58.

[12] C.J. Liang, W.C.H. Choy, Color tunable organic light-emitting diodes by using europium organometallic complex, Appl. Phys. Lett. 89 (25) (2006) 251108.

[13] U. Giovanella, M. Pasini, C. Freund, C. Botta, W. Porzio, S. Destri, Highly effi-cient color-tunable OLED based on poly(9,9-dioctylfluorene) doped with a novel europium complex, J. Phys. Chem. C 113 (6) (2009) 2290–2295.

[14] J. Lee, T.-W. Koh, H. Cho, S. Hofmann, S. Reineke, J.-H. Lee, J.-I. Lee, S. Yoo, K. Leo, M.C. Gather, Color temperature tuning of white organic light-emitting diodes via spatial control of micro-cavity effects based on thin metal strips, Org. Electron. 26 (2015) 334–339.

[15] Y. Jiang, J. Lian, S. Chen, H.-S. Kwok, Fabrication of color tunable organic light-emitting diodes by an alignment free mask patterning method, Org. Electron. 14 (8) (2013) 2001–2006.

[16] M. Qian, X.-B. Shi, Y. Liu, Z.-M. Jin, X.-L. Wang, Z.-K. Wang, L.-S. Liao, Theo-retical model for the external quantum efficiency of organic light-emitting diodes and its experimental validation, Org. Electron. 25 (2015) 200–205.

[17] L. Liu, M. Yu, J. Zhang, B. Wang, W. Liu, Y. Tang, Facile fabrication of color-tunable and white light emitting nano-composite films based on layered rare-earth hydroxides, J. Mater. Chem. C 3 (10) (2015) 2326–2333.

[18] T. Xu, L. Yan, J. Miao, Z. Hu, S. Shao, A. Li, I. Murtaza, H. Meng, Unlocking the potential of diketopyrropyrrole-based solar cells by a pre-solvent annealing method in all-solution processing, RSC Adv. 6 (2016) 53587–53595.

[19] S. Liu, J. Li, C. Du, J. Yu, Evaluation and prediction of color-tunable organic light-emitting diodes based on carrier/exciton adjusting interlayer, Appl. Phys. Lett. 107 (4) (2015) 041109.

[20] S.O. Jeon, C.W. Joo, K. Yook, J.Y. Lee, Color control of multilayer stacked white polymer light-emitting diodes using a quantum dot as an interlayer, Appl. Phys. Lett. 94 (9) (2009) 093303.

[21] J.-H. Jou, M.-H. Wu, S.-M. Shen, H.-C. Wang, S.-Z. Chen, S.-H. Chen, C.-R. Lin, Y.-L. Hsieh, Sunlight-style color-temperature tunable organic light-emitting diode, Appl. Phys. Lett. 95 (1) (2009) 013307.

[22] K.S. Yook, C.W. Joo, S.O. Jeon, J.Y. Lee, Small molecule based mixed interlayer for color control of solution processed multilayer white polymer light-emitting diodes, Org. Electron. 11 (2) (2010) 184–187.

[23] M.-H. Huang, W.-C. Lin, C.-C. Fan, Y.-S. Wang, H.-W. Lin, J.-L. Liao, C.-H. Lin, Y. Chi, Tunable chromaticity stability in solution-processed organic light emitting devices, Org. Electron. 20 (2015) 36–42.

[24] K. Xue, R. Sheng, Y. Duan, P. Chen, B. Chen, X. Wang, Y. Duan, Y. Zhao, Efficient non-doped monochrome and white phosphorescent organic light-emitting diodes based on ultrathin emissive layers, Org. Electron. 26 (2015) 451–457.

[25] S. Han, C. Huang, Z.-H. Lu, Color tunable metal-cavity organic light-emitting diodes with fullerene layer, J. Appl. Phys. 97 (9) (2005) 093102.

[26] Y. Yin, J. Yu, H. Cao, L. Zhang, H. Sun, W. Xie, Efficient non-doped phospho-rescent orange, blue and white organic light-emitting devices, Sci. Rep. 4 (2014) 6754.

[27] Y.-L. Chang, Y. Song, Z. Wang, M.G. Helander, J. Qiu, L. Chai, Z. Liu, G.D. Scholes, Z. Lu, Highly efficient warm white organic light-emitting diodes by triplet exciton conversion, Adv. Funct. Mater. 23 (6) (2013) 705–712.

[28] G.L. Ingram, Z.-H. Lu, Design principles for highly efficient organic light-emitting diodes, J. Photonics Energy 4 (1) (2014), 040993–040993.

[29] J.-H. Jou, S.-M. Shen, C.-R. Lin, Y.-S. Wang, Y.-C. Chou, S.-Z. Chen, Y.-C. Jou, Efficient very-high color rendering index organic light-emitting diode, Org. Electron. 12 (5) (2011) 865–868.

[30] M. Yang, W. Jing, Shi Xindong, Jun Liu, Xinkai Wu, Yang Wang, Zhiyuan Min, Gufeng He, Color-stable and low-roll-off fluorescent white organic light emitting diodes based on nondoped ultrathin emitters, Sci. Adv. Mater. 8 (6)

[31] Z. Tianhang, C.H.C. Wallace, High-efficiency blue fluorescent organic light emitting devices based on double emission layers, J. Phys. D: Appl. Phys. 41 (5) (2008) 055103.

[32] P.G. Wu, L. Brand, Resonance energy transfer: methods and applications, Anal. Biochem. 218 (1) (1994) 1–13.

[33] G.D. Scholes, Long-range resonance energy transfer in molecular systems, Annu. Rev. Phys. Chem. 54 (1) (2003) 57–87.

[34] A. Olaya-Castro, G.D. Scholes, Energy transfer from Förster–Dexter theory to quantum coherent light-harvesting, Int. Rev. Phys. Chem. 30 (1) (2011) 49–77.

[35] S. Jang, M.D. Newton, R.J. Silbey, Multichromophoric F\"orster resonance en-ergy transfer, Phys. Rev. Lett. 92 (21) (2004) 218301.

[36] S. Jang, M.D. Newton, R.J. Silbey, Multichromophoric förster resonance energy transfer from B800 to B850 in the light harvesting complex 2: evidence for subtle energetic optimization by purple bacteria, J. Phys. Chem. B 111 (24) (2007) 6807–6814.

[37] B.W. Van der Meer, G. Coker, S.Y.S. Chen, Resonance Energy Transfer: Theory and Data, VCH, New York, 1994.

[38] H.-C. Chen, C.-Y. Hung, K.-H. Wang, H.-L. Chen, W.S. Fann, F.-C. Chien, P. Chen, T.J. Chow, C.-P. Hsu, S.-S. Sun, White-light emission from an upconverted emission with an organic triplet sensitizer, Chem. Commun. 27 (2009) 4064–4066.

[39] A. Monguzzi, J. Mezyk, F. Scotognella, R. Tubino, F. Meinardi, Upconversion-induced fluorescence in multicomponent systems: steady-state excitation power threshold, Phys. Rev. B 78 (19) (2008) 195112.

[40] J.D. Axe, P.F. Weller, Fluorescence and energy transfer in Y2O3:Eu3+, J. Chem. Phys. 40 (10) (1964) 3066–3069.

[41] J. Eisinger, B. Feuer, A.A. Lamola, Intramolecular singlet excitation transfer. Applications to polypeptides, Biochemistry 8 (10) (1969) 3908–3915.

[42] V. Jankus, K. Abdullah, G.C. Griffiths, H. Al-Attar, Y. Zheng, M.R. Bryce, A.P. Monkman, The role of exciplex states in phosphorescent OLEDs with poly(vinylcarbazole) (PVK) host, Org. Electron. 20 (2015) 97–102.

[43] Y.-K. Kim, J. Won Kim, Y. Park, Energy level alignment at a charge generation interface between 4,4′-bis(N-phenyl-1-naphthylamino)biphenyl and 1,4,5,8,9,11-hexaazatriphenylene-hexacarbonitrile, Appl. Phys. Lett. 94 (6) (2009) 063305.

[44] Q. Xue, S. Zhang, G. Xie, Z. Zhang, L. Zhao, Y. Luo, P. Chen, Y. Zhao, S. Liu, Efficient fluorescent white organic light-emitting devices based on a ultrathin 5,6,11,12-tetraphenylnaphthacene layer, Solid State Electron. 57 (1) (2011) 35–38.

[45] J.-H. Jou, M.-C. Tang, P.-C. Chen, Y.-S. Wang, S.-M. Shen, B.-R. Chen, C.-H. Lin, W.-B. Wang, S.-H. Chen, C.-T. Chen, F.-Y. Tsai, C.-W. Wang, C.-C. Chen, C.-C. Wang, Organic light-emitting diode-based plausibly physiologically-friendly low color-temperature night light, Org. Electron. 13 (8) (2012) 1349–1355.

[46] J.-H. Jou, H.-C. Wang, S.-M. Shen, S.-H. Peng, M.-H. Wu, S.-H. Chen, P.-H. Wu, Highly efficient color-temperature tunable organic light-emitting diodes, J. Mater. Chem. 22 (16) (2012) 8117–8120.

[47] G. Cheng, K.T. Chan, W.-P. To, C.-M. Che, Color tunable organic light-emitting devices with external quantum efficiency over 20% based on strongly lumi-nescent gold(III) complexes having long-lived emissive excited states, Adv. Mater. 26 (16) (2014) 2540–2546.

[48] K.S. Yook, S.O. Jeon, C.W. Joo, J.Y. Lee, Color stability and suppressed efficiency roll-off in white organic light-emitting diodes through management of interlayer and host properties, J. Ind. Eng. Chem. 15 (3) (2009) 420–422.

[49] Y. Seino, H. Sasabe, Y.-J. Pu, J. Kido, High-performance blue phosphorescent OLEDs using energy transfer from exciplex, Adv. Mater. 26 (10) (2014) 1612–1616.

[50] T. Nakagawa, S.-Y. Ku, K.-T. Wong, C. Adachi, Electroluminescence based on thermally activated delayed fluorescence generated by a spirobifluorene donor-acceptor structure, Chem. Commun. 48 (77) (2012) 9580–9582.